



Interfacial reactions between pure indium solder and Au/Ni metallization

Li-Chi Huang¹, Yan-Ping Zhang¹, Chih-Ming Chen^{1,2,*} , Liang-Yih Hung³, and Yu-Po Wang³

¹Department of Chemical Engineering, National Chung Hsing University, 145 Xingda Rd., South Dist, Taichung 402, Taiwan

²Innovation and Development Center of Sustainable Agriculture (IDCSA), National Chung Hsing University, Taichung 402, Taiwan

³Corporate Research and Development, Siliconware Precision Industries Co. Ltd, Taichung 427, Taiwan

Received: 5 February 2022

Accepted: 11 April 2022

Published online:

2 May 2022

© The Author(s), under exclusive licence to Springer Science+Business Media, LLC, part of Springer Nature 2022

ABSTRACT

Thermal interface material (TIM) attracts considerable attention as the increasing demands for efficient heat dissipation in high-performance microelectronic packages. Due to high thermal conductivity, pure indium is a promising candidate of TIM. The TIM joint between two adjoining components is constructed by solid–liquid interdiffusion (SLID) reaction between indium and Au/Ni metallization on the adjoining surfaces. An understanding of the formation and growth kinetics of the intermetallic compounds (IMCs) at the In/Au/Ni interface is crucial for the reliability assessment of the TIM joints. In this study, the interfacial reactions between indium and Au/Ni in the SLID and thermal aging processes at 220–260 °C and 100–150 °C, respectively, are investigated. The metallographic analysis indicates that the thin Au layer dissolves rapidly into the molten indium matrix, leaving only one IMC at the In/Ni interface in the SLID and aging reactions. Compositional and crystallographic analyses both confirm that the IMC is Ni₂₈In₇₂ incorporated with a small amount of Au solubility. The thickness evolution of Ni₂₈In₇₂ displays a linear relationship with the square root of reaction time, indicating a diffusion-controlled growth behavior.

1 Introduction

With the increasing demands for high performance microprocessors, the number of transistors on the chip increases dramatically and therefore thermal management becomes a critical reliability issue. A heat spreader is commonly used to spread the heat generated from the dies to the surroundings. The

connection between the heat spreader and the silicon dies requires the thermal interface material (TIM) that possesses high thermal conductivity to facilitate the heat dissipation [1, 2]. Another requirement of TIM is the capability of absorbing the thermal strains that result from the mismatch of coefficients of thermal expansion (CTE) at the heterogeneous junctions. Polymer-based TIMs incorporated with conductive

Address correspondence to E-mail: chencm@nchu.edu.tw

fillers have been widely used due to good adhesion and low processing temperatures [3–5]. To fulfil reliable thermal management at high working temperatures, polymer-based TIMs are not qualified and alternatively metallic solders become the promising TIMs due to their higher thermal conductivity and better thermal stability [1, 2, 6–9]. Low melting point pure indium (In) is one of the promising candidates from the perspective of lower processing temperature [7–9].

Implementation of In as the TIM involves a joining process which is accomplished via a solid-liquid interdiffusion (SLID) technique. During the SLID reaction, the molten In wets the surfaces of two adjoining components. To enhance the wettability and solderability, a Au/Ni dual-layer metallization is usually deposited on the surfaces of the adjoining components [10–12]. The joining reactions usually accompany the formation of intermetallic compounds (IMCs) which is considered as a sign of successful joining. However, IMCs with a fast growth rate are undesirable because of their brittle nature [13]. Therefore, an understanding of the formation and growth kinetic of IMCs at the contact interface between In and Au/Ni metallization is essential for the reliability assessment of the TIM joints.

Kim et al. fabricated the reaction couples by joining an In sheet with a Au/Ni substrate at 197 °C, and then investigated the formation and growth of IMCs at the In/Au/Ni interface at temperatures from 70 to 120 °C [14]. The $\text{Ni}_{10}\text{In}_{27}$ phase (also denominated as $\text{Ni}_{28}\text{In}_{72}$ or Ni_3In_7 elsewhere [15]) was found as the main IMC at the joint interface [14], and its growth followed the parabolic law, indicating a diffusion-controlled growth mechanism. The absence of In–Au IMCs at the interface was attributed to the rapid dissolution of the thin Au layer in molten In matrix and its low concentration that hindered the formation of In–Au IMCs. Interfacial reactions between In and Au/Ni(V) surface finish at liquid/solid (220–260 °C) and solid/solid (100–150 °C) state were investigated systematically [15]. The $\text{Ni}_{28}\text{In}_{72}$ phase was also the primary IMC at the joint interface regardless of the reaction temperatures, while an amorphous Ni–V–In phase was formed from the original Ni(V) layer due to outward diffusion of Ni and inward diffusion of In [15]. The reactions between In and Ni without an Au interlayer were also investigated, and the dominant IMC was also the $\text{Ni}_{10}\text{In}_{27}$ phase at the In/Ni

interface at lower reaction temperatures (< 300 °C) [16, 17] but became NiIn and Ni_2In_3 at 500 °C [18].

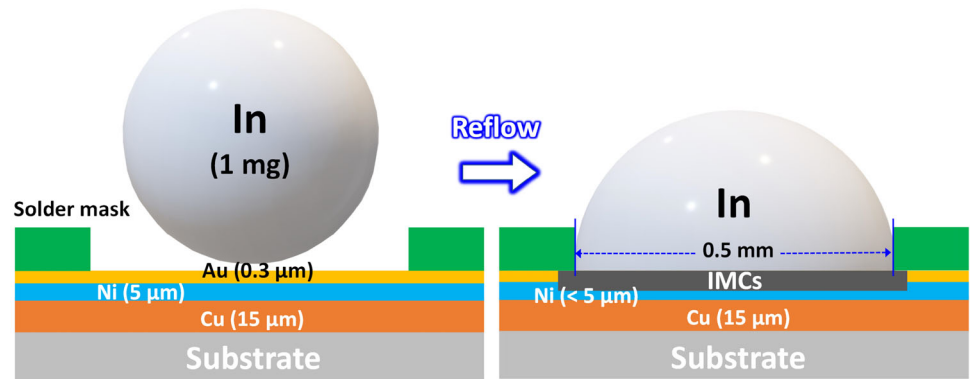
Although the joint of In and Au/Ni is an important system in TIM applications, the study of interfacial reactions between In and Au/Ni is rarely seen [14, 15]. Therefore, it is of significant importance to investigate the IMC formation and their growth kinetics at the In/Au/Ni interface to fulfil the literature completeness. In this study, the dual-layer structure of Au/Ni was deposited on the Cu substrate using electrodeposition and reacted with pure In at various temperatures. Liquid In/solid Au/Ni reactions were conducted at 220–260 °C, while solid In/solid Au/Ni reactions were conducted at 100–150 °C. The formation of IMCs at the In/Au/Ni interfaces and their growth kinetics were investigated to gain a basic understanding of the In/Au/Ni joint system.

2 Experimental procedures

Figure 1 shows the sample configuration and preparation process. The substrate was a polymer board deposited with a 15 µm thick Cu layer using electrodeposition. On the surface of the Cu layer, a 5 µm thick Ni layer and a 0.3 µm thick Au layer were deposited sequentially using electrodeposition. To define the area for joining reaction, the surface of the Au layer was covered by a solder mask with a 0.5 mm diameter aperture. The In ball was prepared from a pure In foil. A small piece of In of 1 mg was cut from the In foil and placed on a glass sheet, followed by heating at 180 °C on a hot plate to transform the solid In piece into a molten ball. After cooling down to room temperature, the solidified ball was placed in the aperture of solder mask. To assist the reaction between In and Au, a tiny drop of sparkle flux [WF-6317, Senju Electronic (Taiwan) Co., Ltd.] was pasted on the exposed Au surface before the placement of the In ball. One of the main functions of flux was to retain clean surfaces of In and Au by removing the oxidants generated in the heating process.

Liquid/solid and solid/solid reactions of the joint samples were performed to investigate the interfacial reactions between pure In and Au/Ni metallization. For the liquid In/solid Au/Ni reaction, the joint samples were placed on a hot plate at 220 °C, 245 °C, and 260 °C, at which the In ball melted and reacted

Fig. 1 Schematic of the configuration of the In/Au/Ni joint



with the Au/Ni metallization. The reaction time periods were from 1 to 15 min for three reaction temperatures. For the solid In/solid Au/Ni reaction, a heating process was carried out at 180 °C for 1 min first to fabricate the In/Au/Ni joint. Then, isothermal aging was conducted in a furnace at different temperatures of 100 °C, 130 °C, and 150 °C for 24–1000 h.

After the liquid/solid and solid/solid reactions, the joint samples were removed from the heating apparatus and examined metallographically. The joint samples were mounted in epoxy resin first. Grinding with SiC sandpaper was performed in a direction perpendicular to the In/Au/Ni interface to expose the cross sections. Polishing with fine Al₂O₃ powders down to 0.05 μm particle size was performed to prepare scratch-free cross sections for microstructural observations. The history of microstructural evolution in the reaction regions was recorded using a field-emission scanning electron microscopy (FE-SEM, ZEISS Ultra Plus). The reaction region was sliced using a focused ion beam (FIB) to prepare the specimen for compositional and crystallographic examinations using a high-resolution transmission electron microscopy (HR-TEM, JEOL JEM-2010). The compositions of IMCs formed at the In/Au/Ni interface were analyzed using energy-dispersive X-ray spectroscopy (EDX) attached to HR-TEM and the phase identification was carried out with the selected-area electron diffraction analysis. The cross-sectional area of IMC was measured using an image software and was divided by the interfacial linear length to acquire the average thickness of IMC.

3 Results and discussion

Two types of reactions were performed for the In/Au/Ni joint system, one was the liquid/solid reaction and the other was the solid/solid reaction. Figure 2 shows the cross-sectional SEM micrographs of the In/Au/Ni joints after the liquid/solid reaction at 220 °C, 245 °C, and 260 °C for 1 min to 15 min. A thin IMC was formed at the interface after initial reaction at 220 °C for 1 min (Fig. 2a). To perform the phase identification of the IMC, the cross section in Fig. 2a was examined using TEM as shown in Fig. 3. Chunk-type IMC was formed at the interface (Fig. 3a) and the corresponding elemental mapping in Fig. 3b and d indicated that the IMC contained mainly Ni, Au, and In. The EDX results of Fig. 3e showed that the IMC contained Ni of 28.3–31.4 at.%, In of 64.9–68.9 at.%, and Au of 2.7–3.7 at.%. The phase diagrams of three binary reaction systems at the In/Au/Ni interface, including In–Au, In–Ni, and Au–Ni, were adopted to identify the phase formation of IMC. The Au–Ni reaction system was neglected because no any IMCs presented in the Au–Ni phase diagram [19]. Ni₂₈In₇₂, Ni₂In₃, NiIn, Ni₁₃In₉, Ni₂In, and Ni₃In are stable IMCs in the Ni–In reaction system [20, 21]. Based on the compositional results (Fig. 3e), the IMC was likely to be the Ni₂₈In₇₂ phase with a small amount of Au solubility. In the In–Au phase diagram [22], the AuIn₂ phase had a composition of In of 66.67 at% which was very close to the composition of the IMC mentioned above (In of 64.9–68.9 at.%). However, the composition of Au (2.7–3.7 at.%) of the IMC was far below the stoichiometric ratio of the AuIn₂ phase and therefore this possibility was excluded. Selected area electron diffraction pattern of the IMC was shown in Fig. 3f. The spots were clear and aligned in a regular manner, indicating a good

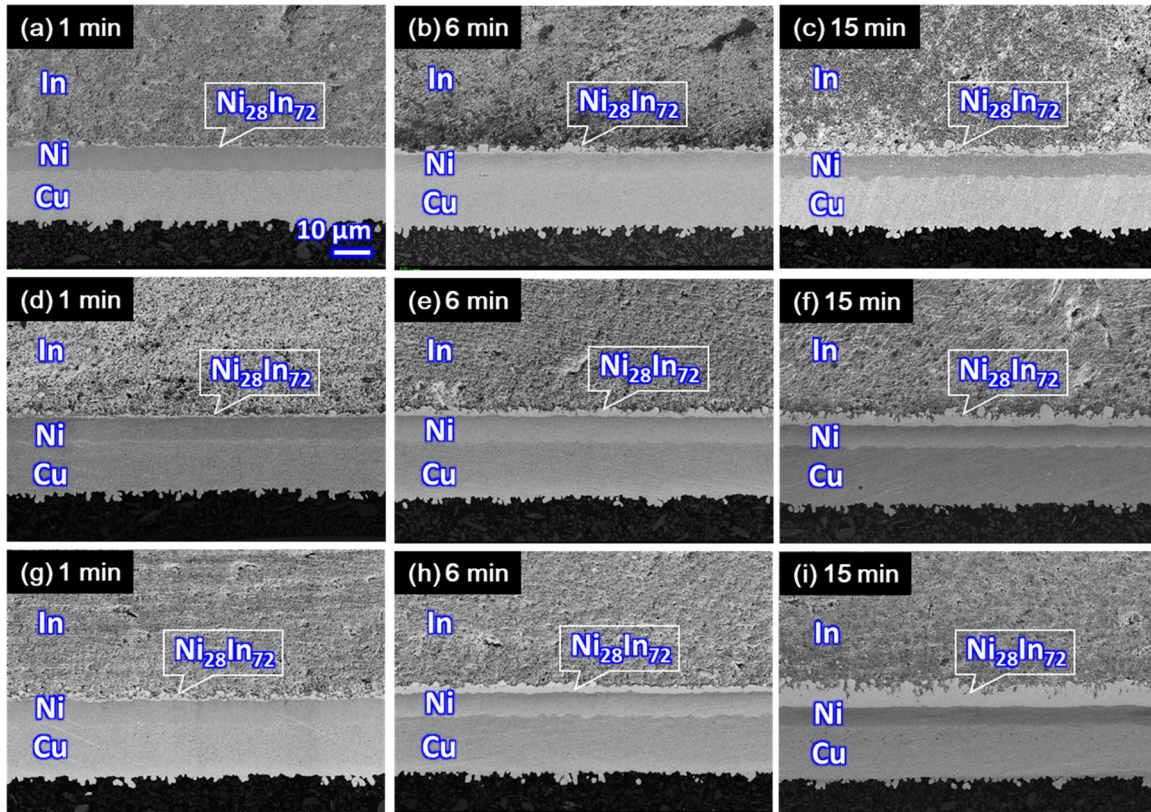


Fig. 2 Cross-sectional SEM micrographs of the In/Au/Ni joints reacted at (a–c) 220 °C, (d–f) 245 °C, and (g–i) 260 °C for 1 min to 15 min

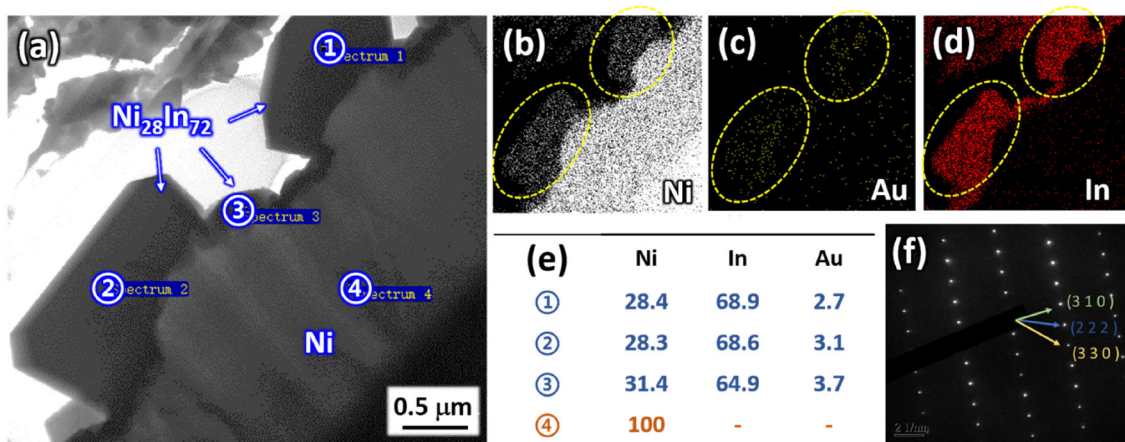


Fig. 3 a Cross-sectional TEM micrograph of the In/Au/Ni joints reacted at 220 °C for 1 min with corresponding elemental mapping of b Ni, c Au, d In, e EDX compositions of atomic

percentage of the reaction zones, f selected area electron diffraction pattern of the reaction product

crystallinity of the IMC and confirming the phase formation of $\text{Ni}_{28}\text{In}_{72}$. The initial thin Au layer at the In/Au/Ni interface was not observed after reaction but a uniform distribution of Au was found in the

$\text{Ni}_{28}\text{In}_{72}$ phase instead. This indicated that the Au layer dissolved into the molten In matrix rapidly and the dissolved atoms were incorporated in the $\text{Ni}_{28}\text{In}_{72}$ phase.

Fig. 4 Cross-sectional TEM micrograph of the In/Au/Ni joints reacted at 260 °C for 15 min: **a** close to the Ni side, **b** close to the In side, **c** EDX compositions of the detection regions in (a) and (b)

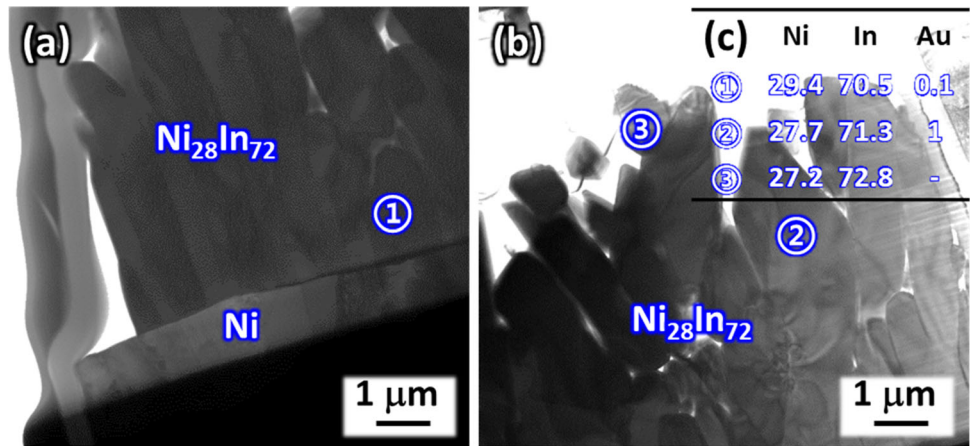
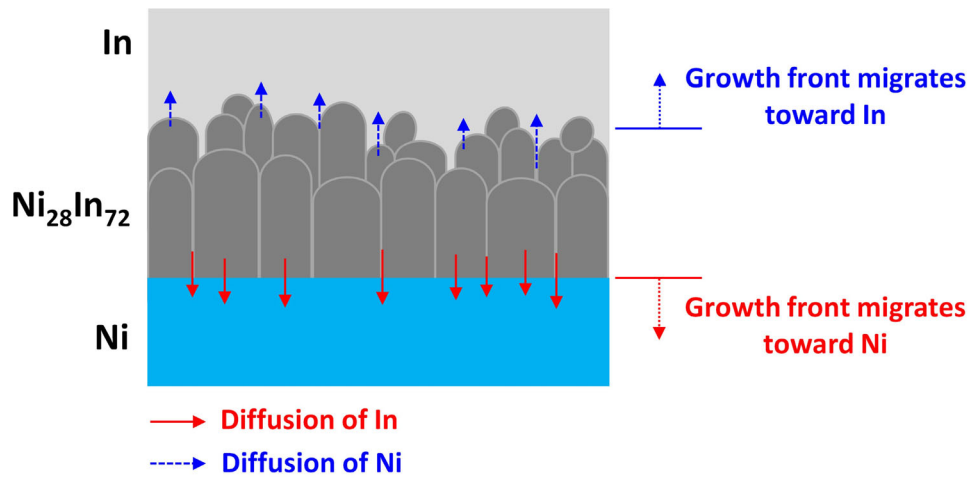


Fig. 5 Schematic of the growth mechanism of the Ni₂₈In₇₂ phase during the liquid/solid reaction



Lee et al. [23] investigated the reactions between molten In-15Pb-5Ag (wt%) solder and Au/Ni/Cu pad at 194 °C. The AuIn₂ phase was observed at the interface in the initial stage of reaction (< 3 min). After reaction for 5 min, the AuIn₂ phase disappeared from the interface and the In-Ni phase was formed instead, but the phase identification was not performed due to a thin thickness. Both the AuIn₂ and Ni₁₀In₂₇ phase were observed at the interface between In solder and Au/Ni/Ti metallizations after rapid thermal annealing at temperatures higher than the melting point of In [24]. Different from the studies mentioned above [23, 24], the AuIn₂ phase was not observed in our study. The discrepancy was attributed to the reaction temperature and the dissolution amount of Au in the molten In matrix. In our study, the liquid/solid reaction was conducted at higher temperatures (220–260 °C) which accelerated the dissolution of Au into the molten In matrix. According to the sample configuration shown in

Fig. 1, the volume of the Au thin layer in the reaction zone was calculated to be $5.89 \times 10^{-8} \text{ cm}^3$. The corresponding amount of Au was $(5.89 \times 10^{-8} \text{ cm}^3) \cdot (19.3 \text{ g/cm}^3) = 1.136 \times 10^{-3} \text{ mg}$. Assuming that all the Au layer was dissolved into the molten In matrix (1 mg), the concentration of Au in the In matrix was estimated to be only 0.1136 wt%. Because the concentration of Au was much lower than its solubility limit ($\sim 1 \text{ wt}\%$) in pure In at the reaction temperatures [22], the AuIn₂ phase was unable to form.

The finding of the primary Ni₂₈In₇₂ phase at the In/Au/Ni interface was in good agreement with our previous study [15]. However, in our previous study [15] the substrate was not pure Ni but a Ni(V) thin layer (0.35 μm) deposited on a Si chip. During the reactions, Ni continued to out-diffuse to participate in the growth of the Ni₂₈In₇₂ phase but the element of V was immobile. On the other hand, the In atoms diffused into the Ni(V) layer and gradually transformed the original crystalline Ni(V) layer into an

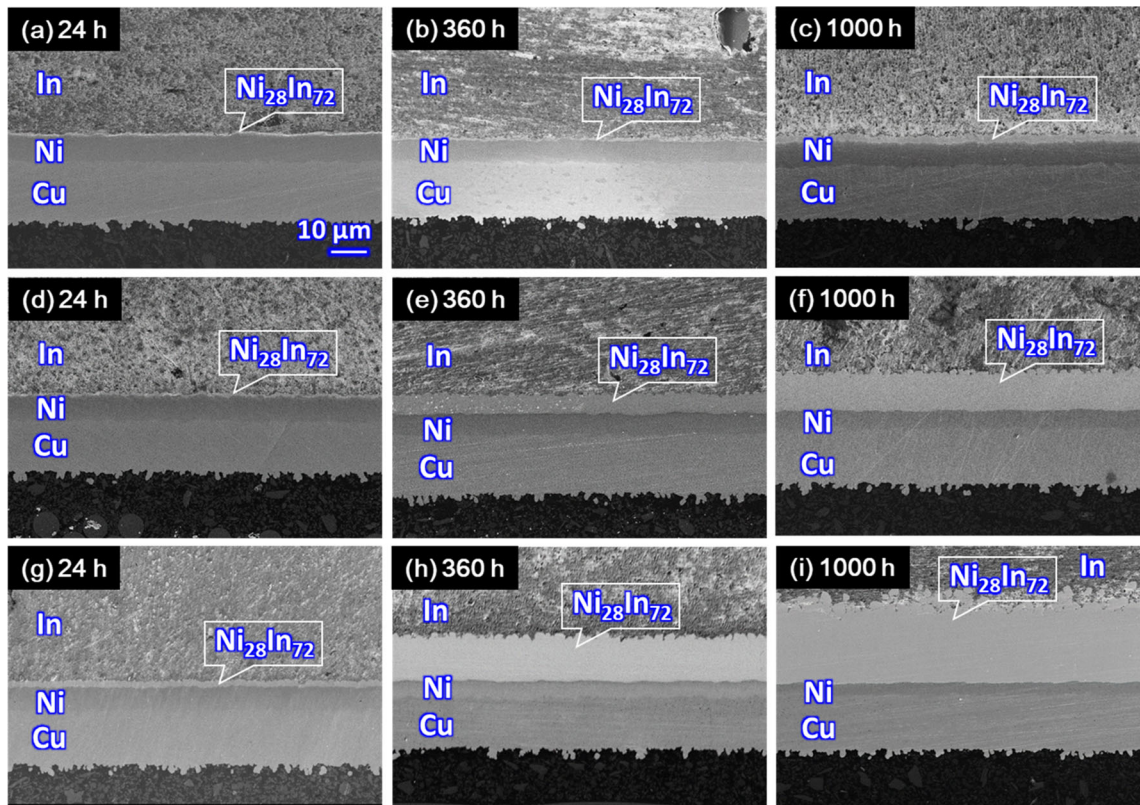


Fig. 6 Cross-sectional SEM micrographs of the In/Au/Ni joints reacted at (a–c) 100 °C, (d–f) 130 °C, and (g–i) 150 °C for 24–1000 h

amorphous Ni–V–In phase. The Ni consumption and phase transformation proceeded at a faster rate in the liquid/solid reaction condition which accelerated the grain spallation of $\text{Ni}_{28}\text{In}_{72}$ from the joint interface. In this present study, the Ni supply was relatively sufficient from a thicker Ni substrate (5 μm) and no Ni–V–In phase presented at the interface. Therefore, only the $\text{Ni}_{28}\text{In}_{72}$ phase was observed and it grew in the form of a layered structure at the In/Ni interface.

As shown in Fig. 2, the $\text{Ni}_{28}\text{In}_{72}$ phase grew in the form of a layer-type structure and its thickness increased with increasing the reaction temperature and time. During the liquid/solid reaction the interface between In and $\text{Ni}_{28}\text{In}_{72}$ displayed a rugged morphology, even after a longer time to 15 min. To observe the interfacial morphology in more details, the cross section in Fig. 2i (260 °C for 15 min) was examined using TEM as shown in Fig. 4. Figure 4a and b show the microstructures of the $\text{Ni}_{28}\text{In}_{72}$ phase close to the Ni side and to the In side, respectively. The $\text{Ni}_{28}\text{In}_{72}$ phase was composed of many column-shaped grains. These grains attached to each other closely at the Ni side (Fig. 4a), giving rise to a compact and planar interface between $\text{Ni}_{28}\text{In}_{72}$ and Ni. By

contrast, the In/ $\text{Ni}_{28}\text{In}_{72}$ interface was rugged due to a loosely packed structure (Fig. 4b). Figure 5 shows the schematic of the growth mechanism of the $\text{Ni}_{28}\text{In}_{72}$ phase during the liquid/solid reaction as mentioned above. According to the mark experiment of Tseng et al. [16], the growth fronts of $\text{Ni}_{28}\text{In}_{72}$ migrated toward Ni and In during the liquid/solid reaction, indicating an interdiffusion process for the growth of $\text{Ni}_{28}\text{In}_{72}$. In other words, the diffusion of both Ni and In contributed to the growth of $\text{Ni}_{28}\text{In}_{72}$. With increasing the thickness of the $\text{Ni}_{28}\text{In}_{72}$ layer, the $\text{Ni}_{28}\text{In}_{72}$ layer acted as a barrier to block the supply of Ni for the growth of $\text{Ni}_{28}\text{In}_{72}$ at the In/ $\text{Ni}_{28}\text{In}_{72}$ interface. As a result, the In/ $\text{Ni}_{28}\text{In}_{72}$ interface evolved into a loosely packed structure as shown in Fig. 4b. The loosely packed structure at the In/ $\text{Ni}_{28}\text{In}_{72}$ interface was also attributed to partial dissolution of the $\text{Ni}_{28}\text{In}_{72}$ grains in molten In or local precipitation of dissolved atoms during the cooling process. The EDX results of Fig. 4c indicated a composition of Ni of 27.2–29.4 at%, In of 70.5–72.8 at%, and Au of 0–1 at%, also confirming the phase formation of $\text{Ni}_{28}\text{In}_{72}$.

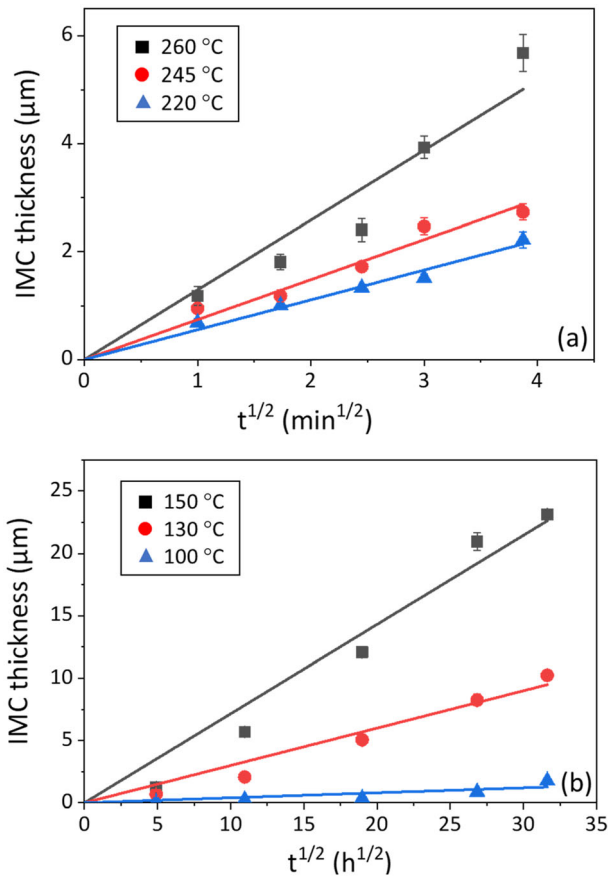


Fig. 7 The relationship between the IMC thickness and the square root of reaction time: **a** liquid/solid reaction and **b** solid/solid reaction. (The straight lines represented the fitting results based on the parabolic law)

Figure 6 shows the cross-sectional SEM micrographs of the In/Au/Ni joints after the solid/solid reaction at 100 °C, 130 °C, and 150 °C for 24 h to 1000 h. The Ni₂₈In₇₂ phase was confirmed as the main IMC at the interface and grew with increasing the reaction temperature and time. The phase formation of Ni₂₈In₇₂ in the solid/solid reaction condition was consistent with the studies previously

reported [23]. Figure 7a and b display the relationship between the Ni₂₈In₇₂ thickness and the square root of reaction time for the liquid/solid and solid/solid reactions, respectively. Basically, the growth of the Ni₂₈In₇₂ phase in the liquid/solid and solid/solid reaction conditions followed the parabolic law because the thickness was approximately proportional to the square root of reaction time as shown by the straight fitting lines. The parabolic growth behavior indicated that the growth of the Ni₂₈In₇₂ phase was diffusion controlled and could be formulated by the equation of $\Delta x = x - x_0 = k t^{1/2}$, where x , x_0 , k , and t are the IMC thickness after reaction, the IMC thickness before reaction, growth rate constant, and reaction time, respectively. Based on the thickness data shown in Fig. 7, the growth rate constant (k) at various reaction temperatures was determined and tabulated in Table 1. As expected, the higher the reaction temperature, the higher the growth rate constant.

The relationship between the growth rate constant and reaction temperature can be formulated by the Arrhenius equation of $k = k_0 \exp(-Q/RT)$, where k_0 , Q , R , and T are temperature-independent prefactor, activation energy, universal gas constant, and absolute temperature, respectively. Plotting the natural logarithm of growth rate constant ($\ln k$) as a linear relationship with the reciprocal of reaction temperature ($1/T$) gave rise to the slope of $-Q/R$ as shown in Fig. 8. As a result, the activation energy (Q) was calculated to be 43.73 kJ/mol and 76.57 kJ/mol for the liquid/solid and solid/solid reactions, respectively. Tseng et al. [16] investigated the growth of the Ni₁₀In₂₇ phase (denominated as Ni₂₈In₇₂ herein) in the liquid In/solid Ni interfacial reactions at temperatures below 300 °C. They reported the activation energy of 94.74 kJ/mol for the Ni₁₀In₂₇ phase which was two times higher than that measured in our study. The discrepancy might be associated with the

Table 1 Growth rate constant and activation energy of the Ni₂₈In₇₂ phase formed in the liquid/solid and solid/solid reactions

	Temperature (°C)	Growth rate constant (μm/min ^{0.5})	Activation energy (kJ/mol)
Liquid/solid reactions	220	0.55385	43.73
	245	0.74145	
	260	1.29364	
Solid/solid reactions	100	0.04008	76.57
	130	0.30002	
	150	0.71574	

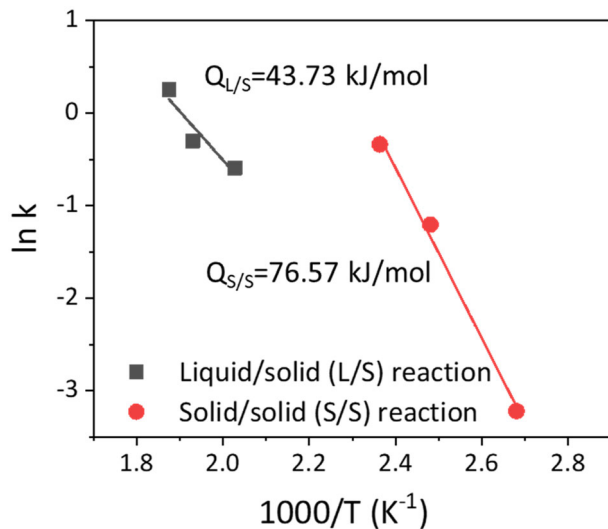


Fig. 8 The relationship between the natural logarithm of growth rate constant ($\ln k$) and the reciprocal of reaction temperature for liquid/solid and solid/solid reactions

Ni source. Tseng et al. used a thicker high-purity Ni plate [16] but the Ni layer in our sample was prepared using electrodeposition. In general, electrodeposition can give rise to a finer grain structure accompanying a high density of grain boundary. The high density of grain boundary in the Ni electroplated layer acted as fast diffusion paths for the atomic interdiffusion and therefore resulted in a lower activation energy. Besides, the growth of the $\text{Ni}_{28}\text{In}_{72}$ phase in this study incorporated with a small amount of Au, and the incorporation of Au might cause the difference of the activation energy.

In our previous study investigating the interfacial reactions between In and Ni(V), the activation energy for the growth of the $\text{Ni}_{28}\text{In}_{72}$ phase was reported to be 13.05 kJ/mol and 47.58 kJ/mol for the liquid/solid and solid/solid reactions, respectively [15]. The two values of activation energy were smaller than those reported in the present study. The discrepancy could also be explained from the viewpoint of microstructure. When the $\text{Ni}_{28}\text{In}_{72}$ phase was formed on the Ni(V) layer, the atomic interdiffusion was enhanced because the Ni(V) layer possessed numerous vertical grain boundaries as the fast diffusivity path. Therefore, the $\text{Ni}_{28}\text{In}_{72}$ phase grew at a faster rate.

4 Conclusions

Liquid/solid and solid/solid reactions between pure In and Au/Ni metallization at 220–260 °C and 100–150 °C, respectively, were performed. In the liquid/solid reaction, the thin Au layer (0.3 μm thick) dissolved rapidly into the molten In matrix in the initial reaction of 1 min at all temperatures. The disappearance of Au allowed the direct reaction of In and Ni, giving rise to the formation of $\text{Ni}_{28}\text{In}_{72}$ at the In/Ni interface. The $\text{Ni}_{28}\text{In}_{72}$ phase incorporated with a small amount of Au solubility became thicker with increasing the reaction temperature and time. A loosely packed structure of the $\text{Ni}_{28}\text{In}_{72}$ phase was observed near the In side after a long-term reaction which was attributed to the deficiency of Ni supply due to the barrier effect of thicker $\text{Ni}_{28}\text{In}_{72}$. Partial dissolution of $\text{Ni}_{28}\text{In}_{72}$ grains and local precipitation of dissolved atoms were also responsible for the loosely packed structure formed at the In/ $\text{Ni}_{28}\text{In}_{72}$ interface. In the solid/solid reaction, the disappearance of Au and the formation of $\text{Ni}_{28}\text{In}_{72}$ were also observed at the In/Ni interface, and the $\text{Ni}_{28}\text{In}_{72}$ phase grew thicker with increasing the reaction temperature and time. The thickness data of $\text{Ni}_{28}\text{In}_{72}$ were recorded as a function of the reaction time for all reaction temperatures, showing that the growth of $\text{Ni}_{28}\text{In}_{72}$ followed the parabolic law and, in other words, a diffusion-controlled mechanism. Based on the growth rate constants obtained from the parabolic growth kinetics, the activation energy of the $\text{Ni}_{28}\text{In}_{72}$ phase was calculated to be 43.73 kJ/mol and 76.57 kJ/mol for the liquid/solid and solid/solid reactions, respectively.

Author contributions

All authors contributed to the study conception and design. Material preparation, data collection and analysis were performed by L-CH and Y-PZ. The first draft of the manuscript was written by C-MC and all authors commented on previous versions of the manuscript. All authors read and approved the final manuscript.

Funding

The authors thank the Siliconware Precision Industries Co., Ltd. for the financial support and offering the materials to prepare the samples. This work was also financially supported by the “Innovation and Development Center of Sustainable Agriculture” from The Featured Areas Research Center Program within the framework of the Higher Education Sprout Project by the Ministry of Education (MOE) in Taiwan.

Data availability

The data generated and/or analysed during the current study are not publicly available for legal/ethical reasons but are available from the corresponding author on reasonable request.

Declarations

Conflict of interest The authors declare that they have no conflict of interest.

References

- D.D.L. Chung, J. Mater. Eng. Perform. **10**, 56–59 (2001)
- J.P. Gwinn, R.L. Webb, Microelectron. J. **34**, 215–222 (2003)
- H. Yan, Y. Tang, W. Long, Y. Li, J. Mater. Sci. **49**, 5256–5264 (2014)
- J. Xu, A. Munari, E. Dalton, A. Mathewson, K.M. Razeeb, J. Appl. Phys. **106**, 124310 (2009)
- H. Ma, B. Gao, M. Wang, Z. Yuan, J. Shen, J. Zhao, Y. Feng, J. Mater. Sci. **56**, 1064–1086 (2021)
- R. Zhang, J. Cai, Q. Wang, J. Li, Y. Hu, H. Du, L. Li, J. Electron. Packag. **136**, 011012 (2014)
- C. Deppisch, T. Fitzgerald, A. Raman, F. Hua, C. Zhang, P. Liu, M. Miller, JOM **58**, 67–74 (2006)
- T. Chaowasakoo, T.H. Ng, J. Songninluck, M.B. Stern, S. Ankiredd: 25th annual IEEE semiconductor thermal measurement and management symposium (SEMI-THERM 2009), 2009, pp. 180–185
- S.S. Too, M. Touzelbaev, M. Khan, R. Master, J. Diep, and K.H. Keok: 25th Annual IEEE semiconductor thermal measurement and management symposium (SEMI-THERM 2009), 2009, pp. 186–192
- C.P. Lin, C.M. Chen, Microelectron. Reliab. **52**, 385–390 (2012)
- Y.W. Yen, Y.C. Chiang, C.C. Jao, D.W. Liaw, S.C. Lo, C. Lee, J. Alloys Compd. **509**, 4595–4602 (2011)
- C.E. Ho, W.T. Chen, C.R. Kao, J. Electron. Mater. **30**, 379–387 (2001)
- P.L. Tu, Y.C. Chan, J.K.L. Lai, IEEE Trans. Compon. Packag. Manuf. Technol.: B **20**, 87–93 (1997)
- D.G. Kim, J.W. Yoon, C.Y. Lee, and S.B. Jung: Mater. Trans. **44**, 72–77 (2003)
- L.C. Huang, Y.P. Zhang, C.M. Chen, L.Y. Hung, Y.P. Wang, Mater. Charact. **184**, 111673 (2022)
- Y.H. Tseng, M.S. Yeh, T.H. Chuang, J. Electron. Mater. **28**, 105–108 (1999)
- S.K. Lin, Y.H. Wang, H.C. Kuo, Intermetallics **58**, 91–97 (2015)
- S.W. Chen, T.C. Yang, J.M. Lin, T.Y. Huang, J. Taiwan. Inst. Chem. Eng. **97**, 356–369 (2019)
- J. Wang, X.G. Lu, B. Sundman, X. Su, Calphad **29**, 263–268 (2005)
- P. Waldner, H. Ipser, Z. Metallkd **93**, 825–832 (2002)
- D. Minić, M. Premović, V. Ćosović, D. Manasijević, L. Nedeljkovic, D. Živković, J. Alloys Compd. **617**, 379–388 (2014)
- H. Okamoto, J. Phase Equilib. Diffus. **25**, 197–198 (2004)
- J.H. Lee, Y.S. Eom, K.S. Choi, B.S. Choi, H.G. Yoon, J.T. Moon, Y.S. Kim, J. Electron. Mater. **33**, 277–282 (2004)
- K. Shin, W.G. Cho, Y.H. Kim, J. Electron. Mater. **32**, 483–491 (2003)

Publisher’s note Springer Nature remains neutral with regard to jurisdictional claims in published maps and institutional affiliations.